Free-Energy Landscapes and Surface Dynamics in Methane Activation on Ni(511) via Machine Learning and Enhanced Sampling

Supporting Information

Yezhi Jin,[†,⊥] Yinan Xu,[*,†,⊥] Jireh S. García Sánchez,[†] Gustavo R. Pérez-Lemus,[†] Pablo F. Zubieta Rico,[†] Massimiliano Delferro,[‡] and Juan J. de Pablo[*,¶,§,‖]

†*Pritzker School of Molecular Engineering, The University of Chicago, 640 S Ellis Ave, Chicago, IL 60637, United States*

‡*Chemical Sciences and Engineering Division, Argonne National Laboratory, 9700 S Cass Ave, Lemont, IL 60439, United States*

¶*Department of Chemical and Biomolecular Engineering, Tandon School of Engineering, New York University, 6 MetroTech Center, Brooklyn, NY 11201, United States*

§*Courant Institute of Mathematical Sciences, New York University, 251 Mercer Street, New York, NY 10012, United States*

‖*Department of Physics, New York University, 726 Broadway, New York, NY 10003, United States*

⊥*These authors contributed equally to this work: Yinan Xu and Yezhi Jin*

E-mail: xuyinan@uchicago.edu; jjd8110@nyu.edu

1 Implementation of the AutoNEB Algorithm

We use the AutoNEB algorithm[1] with the climbing image scheme to identify both the minimum free energy path and the minimum enthalpic path within the collective variable (CV) space. Initially, we generate 20 images through linear interpolation between the initial state (physisorbed methane) and the final state (the adsorbed methyl and hydrogen atom). These images are optimized using the Nudged Elastic Band (NEB) algorithm with a spring constant of 20.0 eV/Å. During the optimization process, we insert additional images every 1000 steps if either the energy difference between two adjacent images exceeds 0.05 eV, or the distance between these images in the CV space is larger than 0.10. The optimization continues for a total of 3000 steps.

2 Free Energy Surface at 1100K

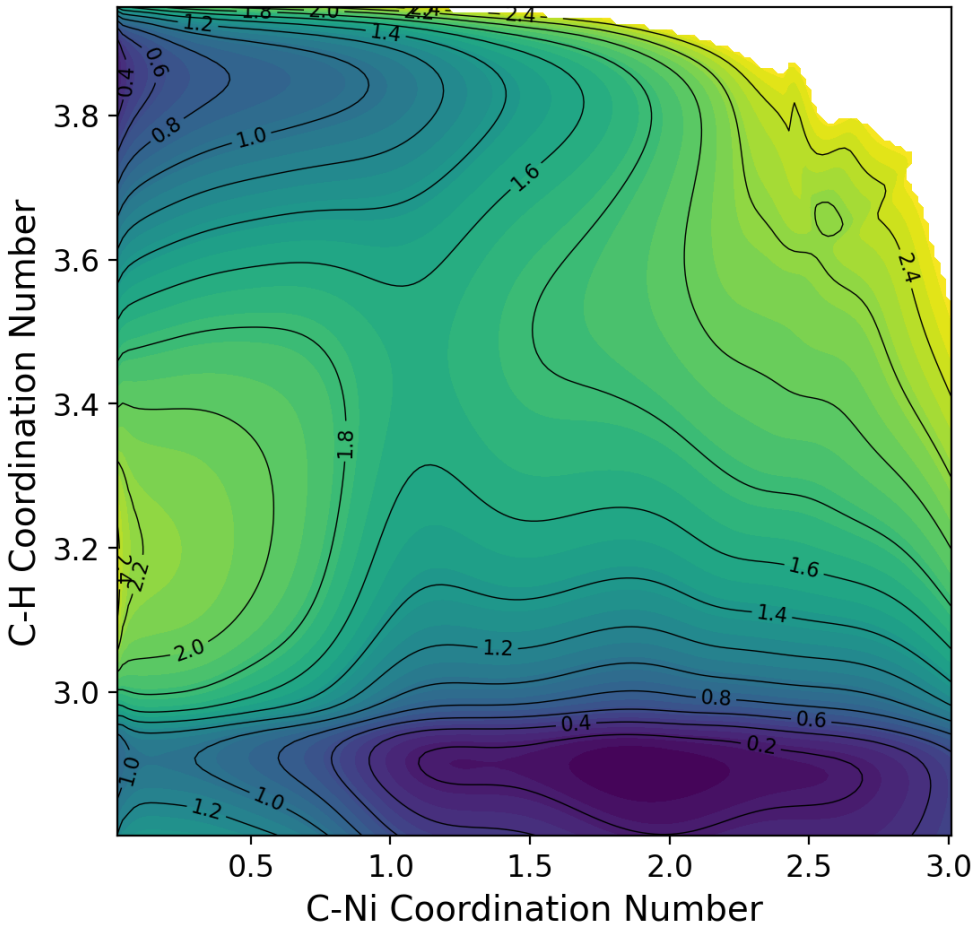

Figure S1: Free energy diagram for methane activation based on MLIP-MD with spectral-ABF sampling scheme, at 1100K.

3 Minimum Free Energy and Enthalpy Paths

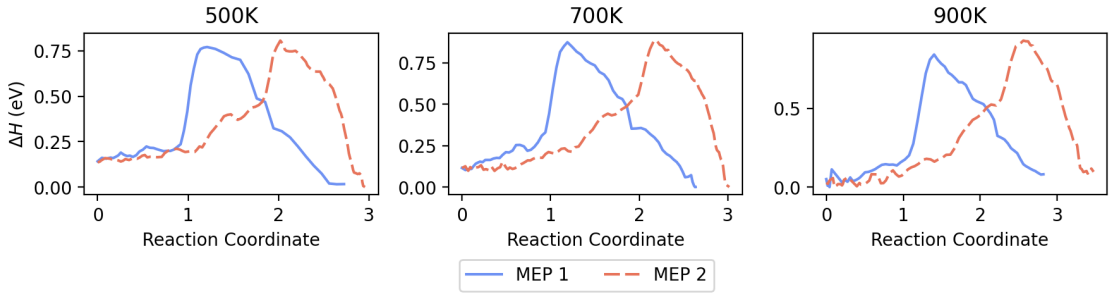

Figure S2: Minimum Enthalpy Path (MEP) 1 and 2 measured by the AutoNEB algorithm with climbing image scheme, under 500K, 700K and 900K. At various temperatures, both MEPs will have a similar height of energy barrier.

Figure S2 shows the profiles of minimum enthalpy paths 1 and 2 for the methane activation routes pointing to the minimum free energy paths (MFEPs) 1 and 2 in Figure 2. These paths are determined using the AutoNEB method at temperatures of 500, 700, and 900 K. For the bridge site-activated route, although its corresponding MFEP2 becomes undetectable at higher temperatures, the path remains observable in the enthalpy profile. Further, the two minimum enthalpy paths maintain similar heights in the activation barrier at all temperatures examined.

4 Convergence Test on Enhanced Sampling

To confirm the convergence of the free energy surface estimated using Spectral-ABF, we perform a convergence test by calculating the root mean squared error (RMSE) of the estimated free energy for each window across consecutive simulation runs. Figure S3 displays the free energy surface estimated by the Spectral-ABF enhanced sampling method[2] for window (2, 3), where the transition state (State 2) is located. This window details the range of Ni—C coordination numbers between 0.595 and 1.285, as well as C—H coordination numbers between 3.25 and 3.55. We observe that the Spectral-ABF method accurately captures the free energy surface within 50 ps of simulation in that window. Figure S4 shows the RMSE values between the free energy estimation of consecutive MD runs. The plateauing of RMSE values between successive runs demonstrates that the free energy estimates have stabilized, confirming that convergence has been achieved.

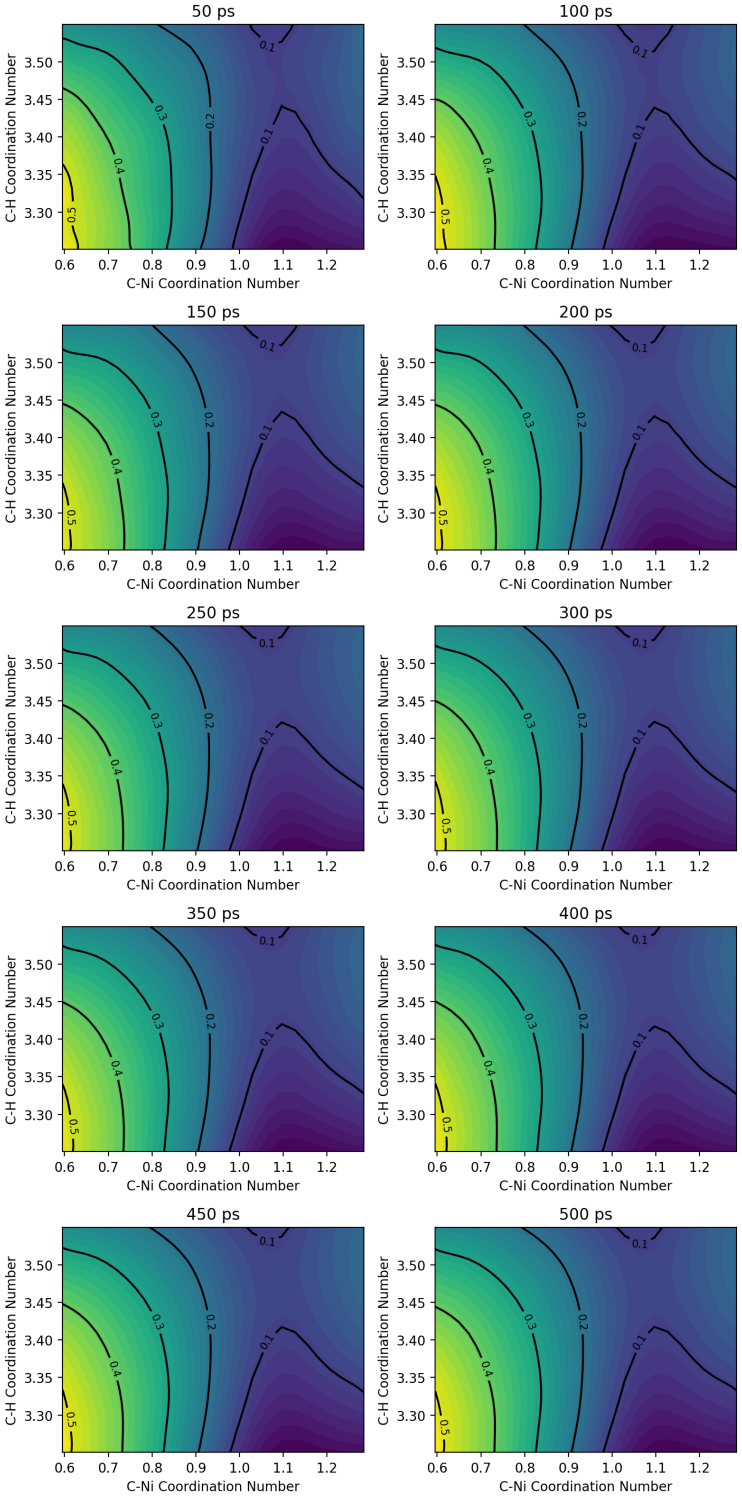

Figure S3: Convergence test of the free energy surface across consecutive simulation runs. The free energy surface shown is the CV window where the transition state resides, with C-Ni coordination number between 0.595 and 1.285, and C-H coordination number between 3.25 and 3.55.

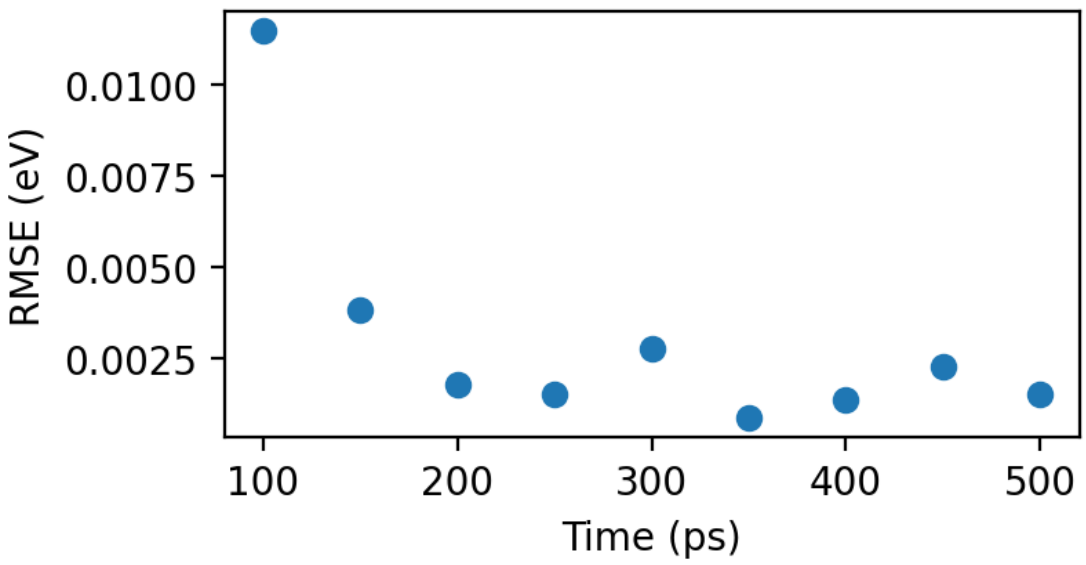

Figure S4: Energy RMSE measured between the free energy surface results of consecutive simulation runs, from the same window as shown in Figure S3.

5 Integration of Gradient Information from Multiple Windows in Enhanced Sampling

To efficiently explore the free energy landscape of methane activation, we partition the collective variable (CV) space into a 5×5 grid, with each grid window further subdivided into 30 bins per axis. Consequently, we perform Spectral-ABF enhanced sampling molecular dynamics (MD) simulations independently within each grid window, yielding gradient estimations of size 30×30 for each window. To integrate the results across all grid windows, we combine these gradient estimations into a complete free energy gradient map of size 150×150, corresponding to the entire CV space (5 windows $\times$ 30 bins per axis = 150 bins per axis). Finally, we fit Chebyshev polynomials to the aggregated gradient map, ensuring that the polynomial gradients accurately reproduce the estimated gradients across the entire CV landscape. This polynomial fitting facilitates a smooth and continuous representation of the free energy surface.

6 Details on Nickel Atom Elevation in Transition States

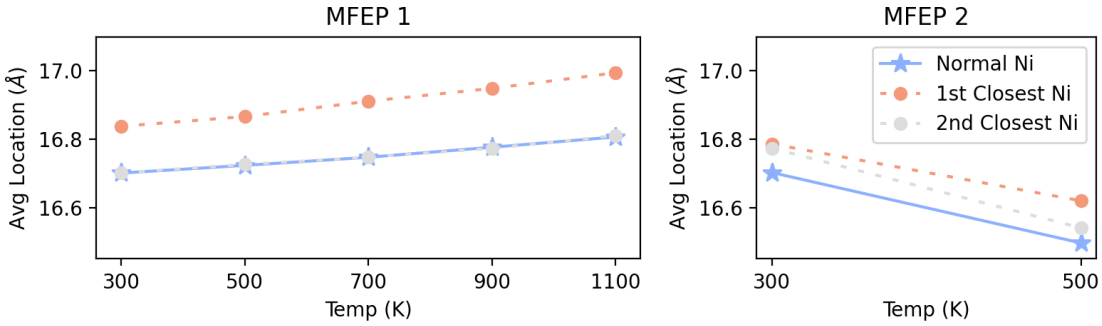

Figure S5: Temperature-dependent z-axis displacement of step site Ni atoms at the methane activation transition state.

Figure S5 quantifies the elevation of nickel atoms from the average surface level in the transition states for both Minimum Free Energy Paths (MFEPs) 1 and 2. Along MFEP2, where two nickel atoms equally participate in the activation process, each nickel atom exhibits a reasonable elevation of 0.03 Å. This elevation is less pronounced compared to the single-atom activation observed along MFEP1, where the nickel atom rises by approximately 0.07 Å at lower temperatures, increasing to over 1.00 Å at 1100 K. This temperature-dependent elevation reflects the enhanced flexibility of the nickel surface, which dynamically adapts to create under-coordinated environments even on terrace sites. This adaptability facilitates localized bond-breaking events, making such under-coordinated states increasingly favorable at higher temperatures. Consequently, the ability of nickel atoms to elevate and create these environments contributes to the reduced free energy gap observed between step and terrace regions for the binding of methane/methyl.

7 Free energy details of the $*CH_3 \rightarrow *CH_2 + H*$ Reaction

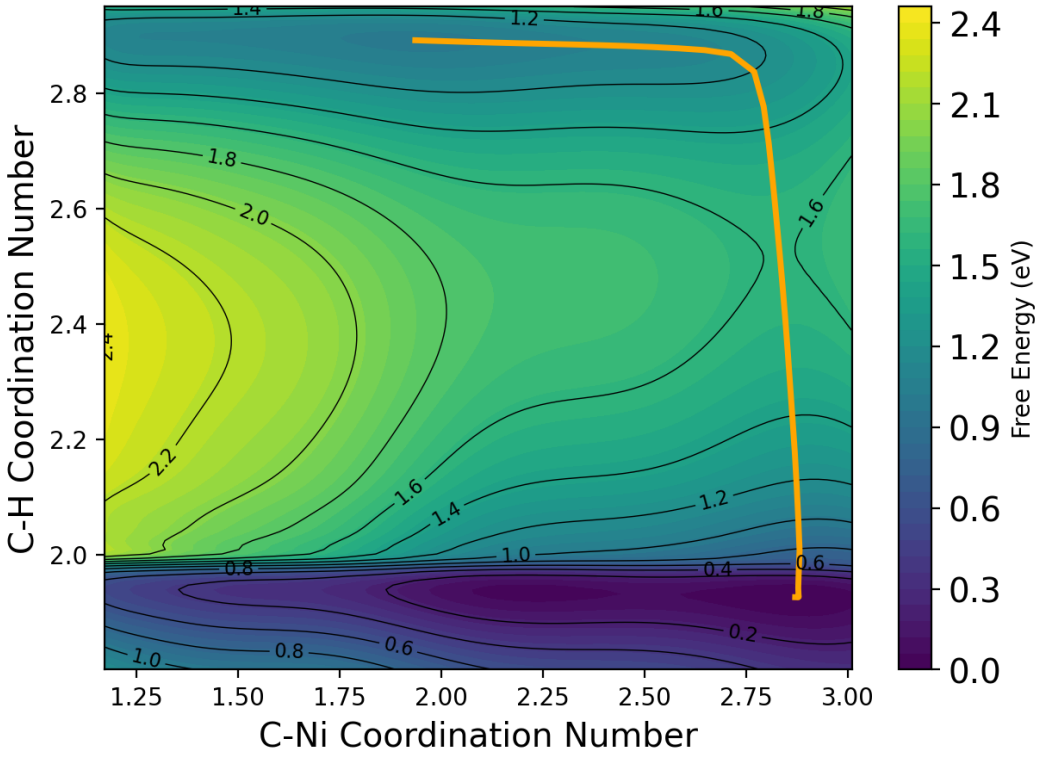

Figure S6: Two-dimensional free-energy surface (FES) for the $^*CH_3 + ^* \rightarrow ^*CH_2 + H^*$ reaction on Ni(511) at 900 K, obtained from molecular dynamics simulations using MLIP optimized for this specific reaction.

8 Visualization of Collective Variables

Figure S7 visualizes the correspondence of the C-H/C-Ni coordination number collective variables, and the Minimum Image Convention (MIC) distances between atoms.

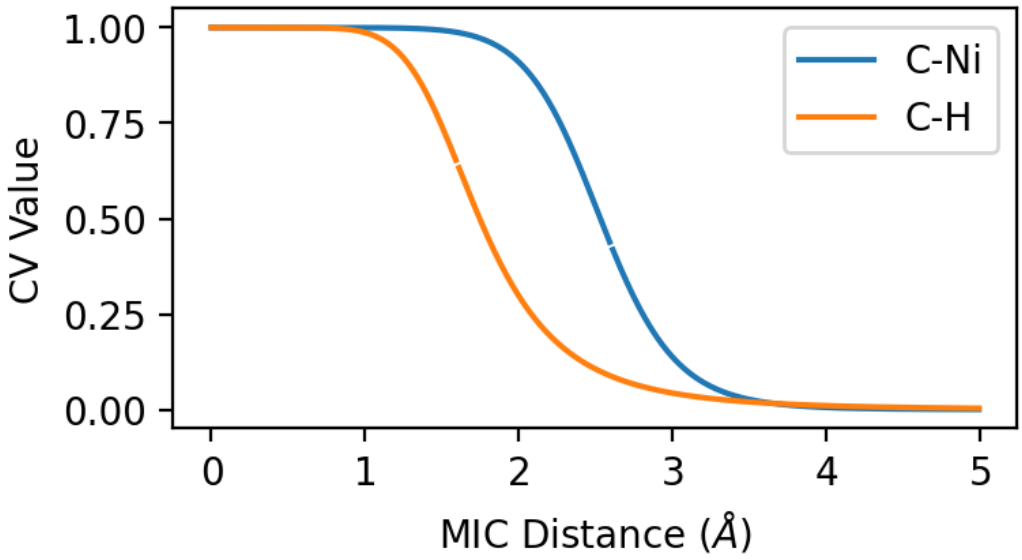

Figure S7: Definition of the C-Ni coordinate number and C-H coordinate number with respect to atom distance.

Supplementary References

(1) Kolsbjerg, E. L.; Groves, M. N.; Hammer, B. An automated nudged elastic band method. *The Journal of chemical physics* **2016**, *145*, 094107.

(2) Zubieta Rico, P. F.; Schneider, L.; Pérez-Lemus, G. R.; Alessandri, R.; Dasetty, S.; Nguyen, T. D.; Menéndez, C. A.; Wu, Y.; Jin, Y.; Xu, Y.; others PySAGES: flexible, advanced sampling methods accelerated with GPUs. *npj Computational Materials* **2024**, *10*, 35.